Clustered-Dot Color Halftone Watermarks using Spatial Frequency and Color Separability

Basak Oztan and Gaurav Sharma

ECE Dept., University of Rochester, Rochester, NY, USA, 14627-0126

ABSTRACT

A framework for clustered-dot color halftone watermarking is proposed. Watermark patterns are embedded in the color halftone on per-separation basis. For typical CMYK printing systems, common desktop RGB color scanners are unable to provide the individual colorant halftone separations, which confounds per-separation detection methods. Not only does the K colorant consistently appear in the scanner channels as it absorbs uniformly across the spectrum, but cross-couplings between CMY separations are also observed in the scanner color channels due to unwanted absorptions. We demonstrate that by exploiting spatial frequency and color separability of clustered-dot color halftones, estimates of the individual colorant halftone separations can be obtained from scanned RGB images. These estimates, though not perfect, allow per-separation detection to operate efficiently. The efficacy of this methodology is demonstrated using continuous phase modulation for the embedding of per-separation watermarks.

Keywords: Color halftone watermarking, color print watermark, color halftone estimation

1. INTRODUCTION

Digital watermarks have recently emerged as an important enabling technology for security and forensics applications for multimedia[1,2] and for hardcopy.[3,4] In the hardcopy domain these techniques provide functionality that mimics or extends the capabilities of conventional paper watermarks that have been extensively utilized since their introduction in the late thirteenth century.[5]

Since most of the hardcopy reproduction relies on the halftone printing, methods that embed the watermark in the halftone structure comprise one of the primary categories of hardcopy digital watermarks. These methods allow printed images to carry watermark data in the form of changes in the halftone structures, which are normally imperceptible but can be distinguished by appropriate detection methods. A number of techniques have been proposed in this area for black and white, i.e., monochrome, printing systems,[6–10] most of which do not directly generalize to color. Thus, there is an unmet need for color halftone watermarking techniques. This need is exacerbated by the fact that image content is often printed in color, particularly as color printing systems become more affordable and accessible.

Sequential printing of individual colorant separations enables per-channel embedding of watermark patterns as in the monochrome case. In order to detect the watermark patterns, one would like to acquire the constituent halftone separations used in the color printing system. For this purpose, ideally, a scanner with K color channels, where each color channel captures only one of the K colorants used in the printing system, is sufficient. However, in actual practice, desktop scanners commonly use RGB color filters to capture color. For a typical CMYK printing system, they are unable to provide the individual halftone separations since: i) Black (K) colorant absorbs uniformly across the spectrum and, thus, it consistently appears in the scanner RGB channels, and ii) so-called "unwanted absorptions" of the CMY colorants cause cross-coupling, i.e., C, M, and Y halftone separations not only appear in the scan R, G, and B channels that complement their spectral absorption bands, respectively, but also in the two other channels as well, between the different colorant halftones in the scanner RGB channels. Therefore, scan RGB channels cannot be readily used for the detection of watermarks embedded in the individual CMYK halftone separations.

Send correspondence to B. Oztan: E-mail: basak.oztan@rochester.edu, Telephone: 1 585 275 8122.

This work is partly supported by a grant from New York State Office of Science, Technology, and Academic Research (NYSTAR) through the Center for Electronic Imaging Systems (CEIS) of University of Rochester.

Color Imaging XV: Displaying, Processing, Hardcopy, and Applications, edited by Reiner Eschbach, Gabriel G. Marcu, Shoji Tominaga, Alessandro Rizzi, Proc. of SPIE-IS&T Electronic Imaging, SPIE Vol. 7528, 75280Y · © 2010 SPIE-IS&T
CCC code: 0277-786X/10/$18 · doi: 10.1117/12.839293

By considering the spectral characteristics of the colorants along with the spatial (frequency) behavior of their halftones, we demonstrate a framework that allows extension of black and white halftone watermarking methods to color on a per-channel basis. Note that dot-on-dot[11] color halftone watermarking may be viewed as an alternate, though rather restrictive, framework for extending black and white watermarking methods to color.[12] In this paper, we consider a general framework for rotated clustered-dot color halftones, which are widely used in practice. Specifically, we exploit the fact that, when suitably designed, the halftones for different colorants can be separated in 2-D spatial frequency despite the couplings in the scan RGB channels. Thus, by utilizing the differences in the spatial frequencies and spectral characteristics, we can obtain estimates of the individual separations. These estimates, though not perfect (due to moiré), do allow for a detection of the embedded watermarks on a per-channel basis. We exploit this methodology to extend halftone watermarking using continuous phase modulation that was introduced for monochrome halftones[13] to color halftones. Note that the present work builds upon and extends our prior work in this area[14] that addressed the more limited setting of three color CMY printing.

2. CLUSTERED-DOT COLOR HALFTONE WATERMARKING

For typical CMYK printing, an overall watermark embedding and extraction scheme is illustrated in Fig. 1. The input cover image $I_{C,M,Y,K}(x,y)$ is a contone CMYK image that is typically obtained by transforming contone RGB color values to CMYK via a set of color conversions.[15] The watermark w_i for the i^{th} colorant separation $I_i(x,y)$, where i is one of C, M, Y, or K, is embedded in the halftone separation $I_i^h(x,y)$ during the halftoning stage. The color halftone image $I_{C,M,Y,K}^h(x,y)$ is obtained by printing the constituent halftone separations in overlay. For the detection of the watermark patterns embedded in these separations, scans of the printed image are obtained using a conventional RGB scanner. Couplings between the CMYK halftone separations are encountered in the RGB channels of the scanned image.

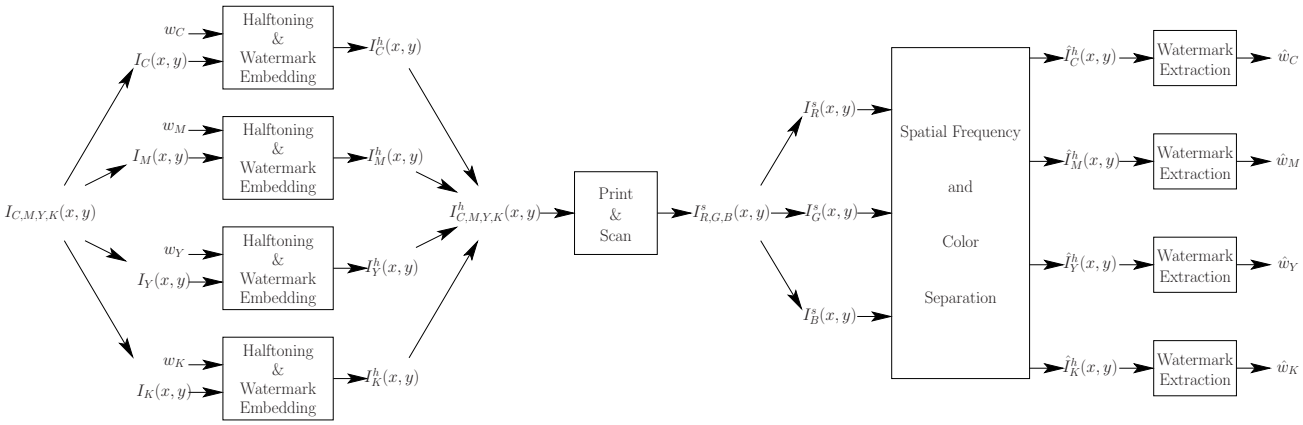

Figure 1. Overview of per-channel basis clustered-dot color halftone watermarking by exploiting spatial frequency and color separation principle.

In order to obtain estimates of the 4 constituent halftone separations from these 3 channels, additional information is required. Here, we rely on the spatial and spectral characteristics of the halftones to provide a solution to this problem. If the halftone frequencies are suitably chosen, spatial filtering and color separability principle (described in greater detail in Sec. 3) can be utilized to "clean" out unwanted halftone structures from the R, G, and B channels of the scanned image to obtain estimates of the C, M, Y, and K halftone separations. For purpose of illustration, Fig. 2(c) later in this paper shows an enlarged view of the G channel of a scanned image from the experimental data to test our framework (the experimental setup will be described later in Sec. 5). An estimate of the M halftone separation as shown in Fig. 2(d) can be obtained using our methodology by removing the unwanted halftone C, Y, and K halftone structures from Fig. 2(c).

Once the (clean) estimate $\hat{I}_i^h(x,y)$ is obtained for the i^{th} colorant halftone, the monochrome watermark detection method can be applied to the separation in order to recover (an estimate of) the corresponding watermark w_i.

3. HALFTONE SEPARATION ESTIMATION EXPLOITING SPATIAL FREQUENCY AND COLOR SEPARABILITY

Our goal is to obtain estimates of the CMYK halftone separations $\hat{I}_i^h(x,y)$, $i \in \{C,M,Y,K\}$, from scan RGB channels of printed images $\hat{I}_i^s(x,y)$, $i \in \{R,G,B\}$. Halftone separation estimate $\hat{I}_i^h(x,y)$ for the i^{th} colorant is a binary image, where the values 1 and 0 correspond to the respective decisions that ink/toner i is, or is not, deposited at the pixel position (x,y). On the other hand, the image $\hat{I}_i^s(x,y)$ from the i^{th} scanner color channel is a contone image, where the image value at pixel position (x,y) represents the fraction of the light reflected from the pixel (x,y) within the transmittance band of the filter i. In the typical 8-bit per-pixel per-color channel representation in RGB scanners, $I_i^s(x,y)$ takes integer values between 0 and 255, where the values 0 and 255 represent the minimum and maximum intensities, respectively.

As we pointed out earlier, for typical desktop RGB scanners, coupling between the different colorant halftones in the scanned RGB image is inevitable. Figure 2(a) shows an enlarged view of a region from the M halftone separation and Fig. 2(b) shows the corresponding view from the corresponding digital CMYK halftone separation overlay, which we use in our experiments to test our framework. In Fig. 2(c), we show the corresponding region from the G channel $I_G^s(x,y)$ of the scanned RGB image $I_{R,G,B}^s(x,y)$. It is apparent that not only is the halftone structure of the desired M channel visible, but due to the fact that the C, Y, and K separations also have absorption in the green scanner channel band, we can also see the undesired halftone structure for these separations in the G channel with varying intensities. This interference can be also observed in the frequency domain. Figure 3 shows enlarged view of the log-magnitude Fourier spectrum of the G channel image for the experimental data around low frequency regions. It can be observed that the Fourier spectrum exhibits peaks not only about the fundamental frequency vectors (and higher-order harmonics) of the M separation, but also at the fundamental frequency vectors of C, Y, and K separations, and moiré frequencies. We exploit the fact that, when suitably designed, these frequencies appear at distant locations in the frequency domain and unwanted frequency components can be eliminated by spatial filtering.

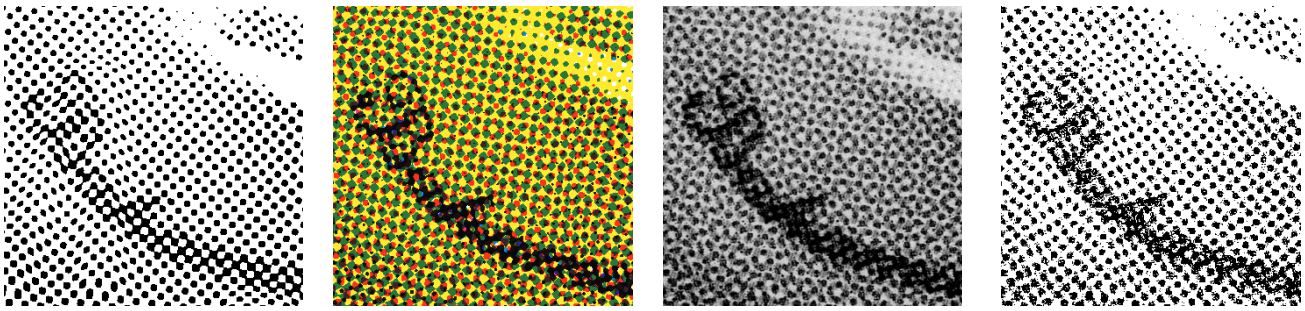

(a) $I_M^h(x,y)$ (b) $I_{C,M,Y,K}^h(x,y)$ (c) $I_G^s(x,y)$ (d) $\hat{I}_M^h(x,y)$

Figure 2. Subfigure (a) shows enlarged view of a region from the digital M halftone separation, subfigure (b) shows enlarged view of the corresponding region from the digital CMYK halftone overlay, subfigure (c) shows the corresponding view from the scanned G channel image $I_G^s(x,y)$ showing the coupling between the halftone structures from M separation and C, Y, and K separations, and subfigure (d) shows enlarged view of the corresponding M halftone estimate.

Spatial filtering may be efficiently implemented by utilizing the 2-D Fast Fourier Transform (FFT). Most of the energy carried by the periodic clustered-dot halftones is concentrated in narrow bands around the fundamental screen frequencies and a lower-order harmonics.[16] We, therefore, utilize narrow band-reject filters $H_i(u,v)$ to remove the unwanted frequency components of the i^{th} separation, where u and v represent the frequency coordinates along the horizontal and vertical directions, respectively. Our experimental results indicate that eliminating the unwanted frequency components around a circular neighborhood (typically with a few lpi radius) of the fundamental screen frequencies and their second-order harmonics of the unwanted separations enables estimation of the desired halftone separation.

A schematic overview of our algorithm is shown in Fig. 4. We first obtain an estimate of K halftone separation using the scan RGB channel images jointly. Detailed description of this process is presented in Sec. 3.1. Next,

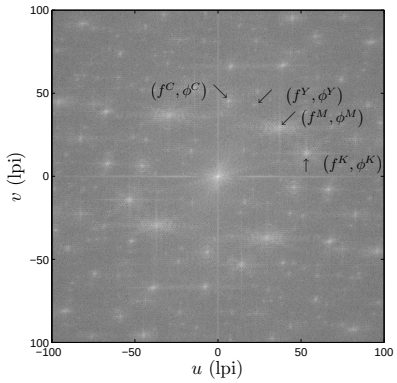

Figure 3. Enlarged view of the *log*-magnitude Fourier spectrum of $I_G^s(x, y)$, the green scanner channel image obtained by scanning a periodic clustered-dot color halftone. For illustration purposes, the frequencies of the constituent halftone separations are indicated by arrow and text labels.

K halftone separation estimate is utilized together with each of the R, G, and B scanned channels to obtain estimates of the complementary C, M, and Y halftone separations, respectively. The estimation process of CMY halftone separations is described in detail in Sec. 3.2.

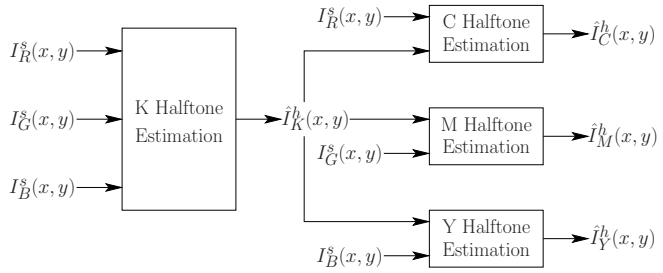

Figure 4. Overview of CMYK halftone separation estimation using the RGB channels of the scanned image.

3.1 Estimation of K Halftone Separation

Since K colorant consistently appears in the scanner RGB channels with similar intensities, all scanner channels are used jointly for the estimation of the K halftone separation. The overall estimation process is illustrated in Fig. 5. Unwanted frequency components of C, M, and Y colorants are removed from the scanner RGB channels by using the band-reject filters $H_j(u, v), j \in \{C, M, Y\}$, as

$$\hat{I}_i^s(x, y) = \mathcal{F}^{-1}\left(\mathcal{F}\left\{I_i^s(x, y)\right\} \prod_{j=C,M,Y} H_j(u, v)\right), \tag{1}$$

where $i \in \{R, G, B\}$, $\mathcal{F}$ denotes the (spatial) Fourier transform operation. The resulting images $\hat{I}_i^s(x, y)$, $i \in \{R, G, B\}$, are then added together in $\hat{I}_K^s(x, y) = \sum_{i=R,G,B} \hat{I}_i^s(x, y)$, and the K halftone separation estimate is finally obtained by

$$\hat{I}_K^h(x, y) = \begin{cases} 1 & \text{if } \hat{I}_K^s(x, y) < \tau_K, \\ 0 & \text{otherwise,} \end{cases} \tag{2}$$

where τ_K is a threshold value.

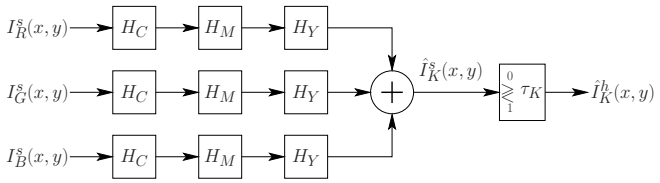

Figure 5. Detailed overview of K halftone separation estimation using spatial filtering.

3.2 Estimation of C, M, and Y Halftone Separations

The efficacy of spatial filtering[14] and color separability[12] principle for the estimation of CMY halftone separations from scan RGB channels images has been shown previously CMY printing systems. For CMYK printing, however, K colorant introduces additional challenges because of which these previously proposed methods alone are insufficient to provide accurate estimates.

From a generalized two dimensional Fourier analysis,[17] we know that the overlap of periodic halftone separations are also periodic (with the period of the intersection lattice). Despite the fact that the frequencies corresponding to the halftone separation overlaps are not eliminated by the band-reject filters we described earlier, we observe that the CMY colorants that are covered by the K colorant in the spatial domain are eliminated if the K frequency components are removed from the RGB scans with a corresponding band-reject filter. A similar elimination is also encountered if the K halftone structures are removed using color separation principle alone. This is due to the fact that K colorant and its overlap with other colorants have similar appearances in the spatial domain. We address this problem by utilizing both techniques jointly, where in addition to the scan RGB channel images, we use the K halftone separation estimate for the estimation of the complementary CMY halftone separations, respectively.

A detailed overview of the M halftone separation estimation is illustrated in Fig. 6, other halftone separations can be estimated similarly. The M halftone separation is estimated from its complementary G channel scan and the K halftone channel estimate. First, an estimate of the overlay of M and K halftone separations is obtained by using color separation. According to the Beer-Lambert law,[18] the absorptance of a layer formed by the superimposition of K layers at wavelength λ is given by $A_{1\ldots K}(\lambda) = 1 - \prod_{k=1}^{K}(1 - A_k(\lambda))$, where $A_k(\lambda)$ is the absorptance of the k^{th} layer at wavelength λ. Therefore, it is expected that the absorptance of the Neugebauer primaries that include both M and K is larger than the absorptances of the constituent Neugebauer primaries. In other words, Neugebauer primaries that include both M and K colorants will appear darker than the constituent Neugebauer primaries in the scanned image channels. Using this property, we obtain an estimate of the MK halftone overlay using color separability. Specifically,

$$\hat{I}^h_{M,K}(x,y) = \begin{cases} 1 & \text{if } I^s_G(x,y) < \tau_{MK}, \\ 0 & \text{otherwise,} \end{cases} \tag{3}$$

represents the estimate of the overlay of M and K halftone separations, where τ_{MK} is a threshold value and the values 1 and 0 correspond to the respective decisions that both M and K toners/inks are, or are not, deposited at the pixel position (x, y). This estimate is then subtracted from the previously obtained K halftone separation estimate $\hat{I}^h_K(x,y)$ in order to get an estimate of $\hat{I}^h_{K'}(x,y)$ that represents the pixel positions that are covered by K colorant, but not M.

Next, the unwanted frequency components of C and Y halftone separations are eliminated from the scan G channel image using the band-reject filters H_C and H_Y, respectively, by

$$\hat{I}^s_{M,K}(x,y) = \mathcal{F}^{-1}\left(\mathcal{F}\{I^s_G(x,y)\}\prod_{j=C,Y} H_j(u,v)\right). \tag{4}$$

Figure 7 illustrates the elimination of the unwanted frequency components of C and Y halftone structures in the Fourier spectrum of the G channel of the experimental data using the band-reject filters H_C and H_Y shown in Figs. 13(a) and (c), respectively.

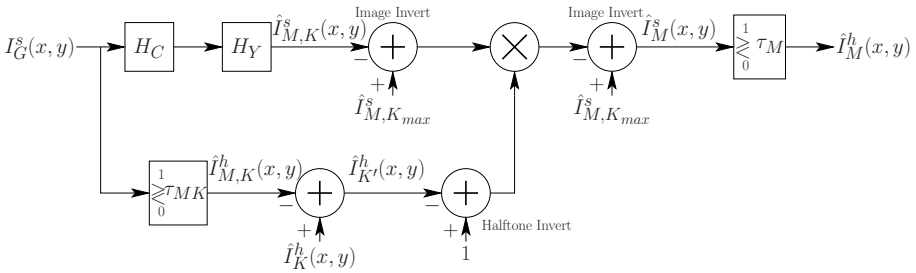

Figure 6. Detailed overview of M halftone separation estimations using spatial filtering and color separation principle.

We then use $\hat{I}^h_{K'}(x,y)$ as a mask to eliminate the K halftone that do not overlap with M from $\hat{I}^s_{M,K}(x,y)$. The elimination is performed by replacing the image values in $\hat{I}^s_{M,K}(x,y)$ with the maximum value $\hat{I}^s_{M,K_{max}}$ of the image where $\hat{I}^h_{K'}(x,y)$ is equal to 1. This can be mathematically expressed as

$$\hat{I}^s_M(x,y) = \hat{I}^s_{M,K_{max}} - \left(\hat{I}^s_{M,K_{max}} - \hat{I}^s_{M,K}(x,y)\right) \times \left(1 - \hat{I}^h_{K'}(x,y)\right). \tag{5}$$

M halftone separation estimate is finally obtained by

$$\hat{I}^h_M(x,y) = \begin{cases} 1 & \text{if } \hat{I}^s_M(x,y) < \tau_M, \\ 0 & \text{otherwise,} \end{cases} \tag{6}$$

where τ_M is a threshold value.

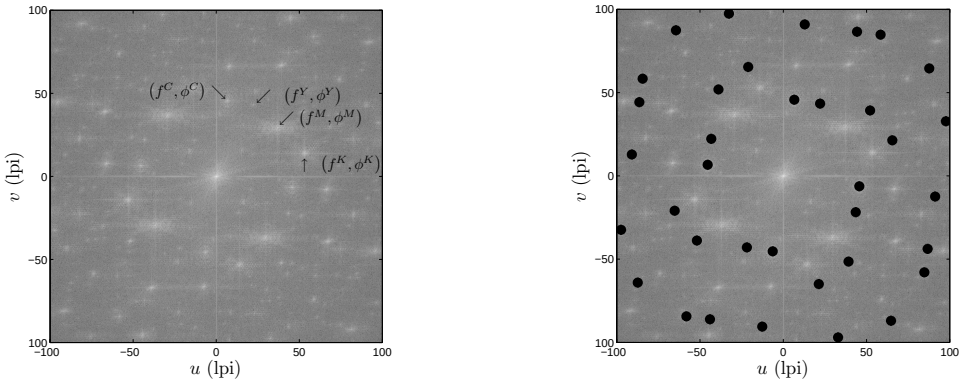

(a) (b)

Figure 7. Subfigure (a) shows enlarged view of the log-magnitude Fourier spectrum of $I^s_G(x,y)$, the green scanner channel image obtained by scanning a periodic clustered-dot color halftone. Subfigure (b) illustrates the elimination of unwanted frequency components of C and Y halftone separations using the band-reject filters shown in Figs. 13(a) and (c), respectively.

The M halftone separation estimate obtained from the enlarged view of the region shown in Fig. 2(c) is shown in Fig. 2(d). The halftone structure of the M separation can be observed much more clearly in Fig. 2(d) in comparison with Fig. 2(c). For purpose of illustration, the images obtained during the estimation of M halftone separation corresponding to the same region are shown in Fig. 8.

3.3 Accuracy of Estimated Halftones

Considering the non-uniformities introduced during the print and scan process, it is difficult to experimentally evaluate the accuracy of the estimation process quantitatively. Therefore, we utilize a simulation framework,

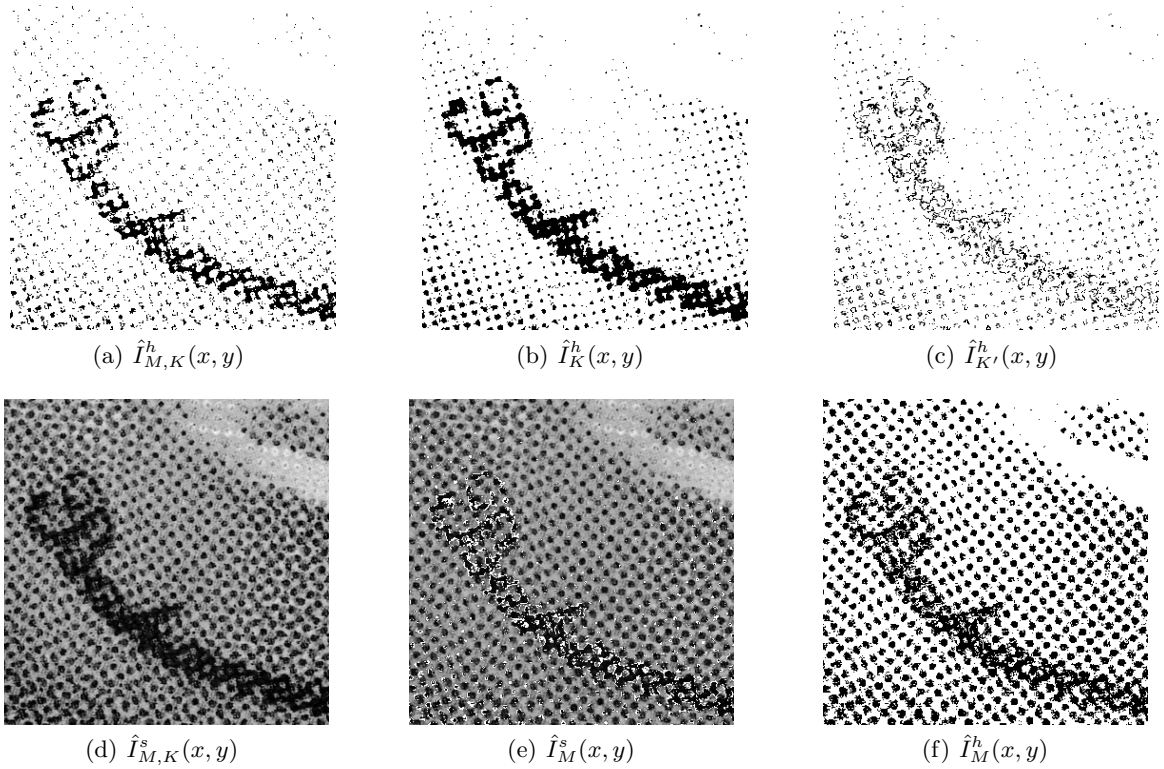

(a) $\hat{I}^h_{M,K}(x,y)$ (b) $\hat{I}^h_{K}(x,y)$ (c) $\hat{I}^h_{K'}(x,y)$

(d) $\hat{I}^s_{M,K}(x,y)$ (e) $\hat{I}^s_{M}(x,y)$ (f) $\hat{I}^h_{M}(x,y)$

Figure 8. Images obtained during the estimation of M halftone separation corresponding to the region shown in Fig. 2(c).

where the effect of print-scan is simulated by the Neugebauer model[18] and spatial blur. The overview of the simulation is shown in Fig. 9. First, individual colorant separation of the contone image $I_{C,M,Y,K}(x,y)$ is halftoned. Next, the effect of the print-scan is simulated on the digital halftone $I^h_{C,M,Y,K}(x,y)$. Estimates of the halftone separations $\hat{I}^h_{C,M,Y,K}(x,y)$ is then obtained from $I^s_{R,G,B}(x,y)$ using our methodology, and, finally, the estimation accuracy for the halftone separation is calculated, details of which are provided subsequently.

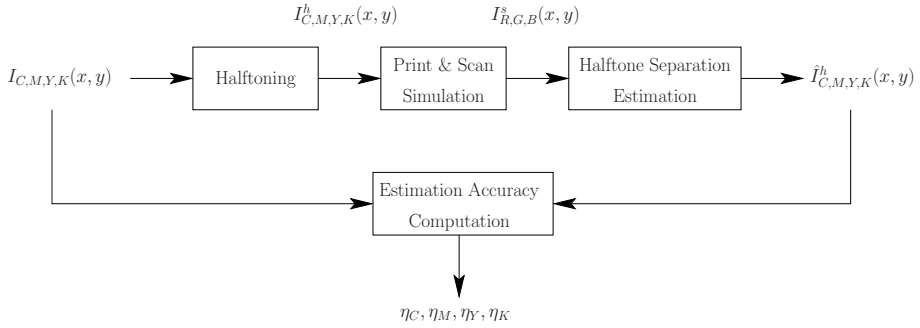

Figure 9. Simulation model for evaluating the accuracy of the estimation process.

We use the image data set shown in Fig. 10 in our simulations. We first generate clustered-dot halftones for these images in 3.84 in $\times$ 2.56 in format for a 600 dpi CMYK color printer. Digital rotated clustered-dot CMYK halftone screens with angular orientations close to the conventional singular moiré-free 15, 75, and 45–deg rotated clustered-dot halftones were utilized for our simulations. For simplicity, we did not embed any watermark pattern in these halftones in our simulations.

(a) *Hats* (b) *Cycles* (c) *Parrots* (d) *Lighthouse*

Figure 10. Contone CMYK image data set used in the simulations.

The effect of print-scan channel is simulated for a 600 dpi CMYK color printer and RGB color scanner combination. In order to simulate the inter-separation colorant interactions,[15] we used the Neugebauer model. Binary CMYK printer values are mapped to contone RGB scanner values through a Look-Up Table (LUT) transformation. For this purpose, average RGB values of 16 Neugebauer primaries[18] for the experimental printer were measured from 0.5×0.5 square-inch printed patches and stored in the LUT. The CMYK values of each pixel in the color halftone are mapped to the RGB scanner values using the LUT. A spatial blur[19] on the individual RGB channels of the resulting image is used to simulate print-scan non-idealities. For this purpose, a 7×7 Gaussian low-pass filter (DC response normalized to 1) with standard deviation approximately equal to 0.96 pixels was employed.

Using the described methodology, we obtain estimates of the individual halftone separations. For purpose of visual comparison, enlarged views of the original CMYK halftone separations and their estimates from a region in the *Hats* image are shown in Fig. 11.

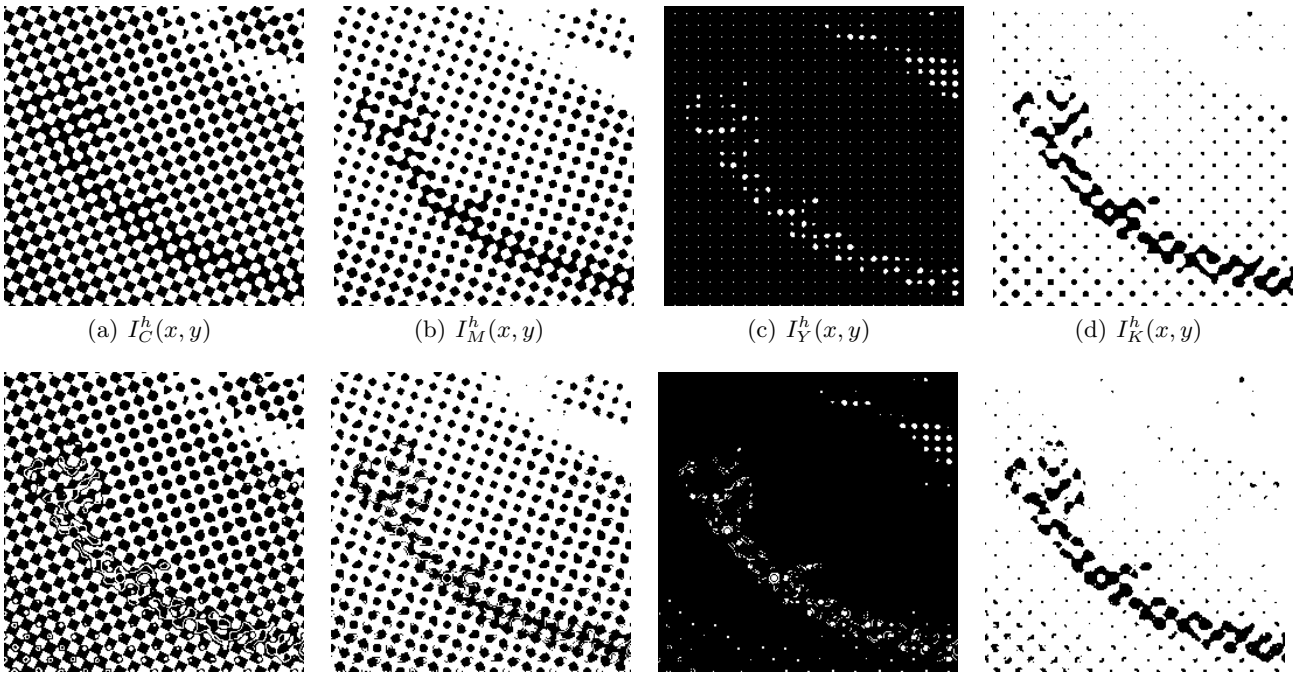

(a) $I_C^h(x,y)$ (b) $I_M^h(x,y)$ (c) $I_Y^h(x,y)$ (d) $I_K^h(x,y)$

(e) $\hat{I}_C^h(x,y)$ (f) $\hat{I}_M^h(x,y)$ (g) $\hat{I}_M^h(x,y)$ (h) $\hat{I}_K^h(x,y)$

Figure 11. Enlarged view of the digital halftone separations from a region in the *Hats* image and their estimates obtained using spatial filtering and color separability.

The accuracy of the described halftone separation estimation methodology is evaluated by the mean absolute difference between the original and estimated halftone image. The percent accuracy for the estimation of the i^{th}

halftone separation is given by

$$\eta_i = \left(1 - \frac{\sum_{x=1}^{M_x}\sum_{y=1}^{M_y} I_i^h(x,y) \oplus \hat{I}_i^h(x,y)}{M_x \times M_y}\right) \times 100, \tag{7}$$

where M_x and M_y are the image dimensions along the horizontal and vertical directions, respectively, and $\oplus$ is the XOR operation. Estimation accuracies for each colorant are listed in Table 1. Around 95% estimation accuracy is achieved for C and K halftone separations and relatively lower accuracies are achieved for the M and Y halftone separations. This difference is caused by different levels of spectral interference observed in the scanner RGB channels. Relatively less interference is observed in the scanner R channel compared to the G and Y channels. Therefore, C and K halftone separations can be estimated better than the M and Y halftone separations. Nevertheless, as we demonstrate later in Sec. 5, these estimates allow successful detection of the embedded watermark patterns.

Image	$\eta_C(\%)$	$\eta_M(\%)$	$\eta_Y(\%)$	$\eta_K(\%)$
Hats	95.9	88.5	87.6	94.3
Cycles	92.1	85.7	84.9	93.7
Parrots	96.0	88.9	89.7	94.7
Lighthouse	95.7	90.4	89.8	95.9

Table 1. Accuracies of halftone separation estimates accuracies by the proposed methodology for the image set shown in Fig. 10.

4. COLOR HALFTONE WATERMARKING USING CONTINUOUS PHASE MODULATION (CPM)

Having described the overall framework in an abstract setting, we next demonstrate a specific and concrete instantiation based on continuous phase modulation (CPM) for monochrome watermark embedding.[13] In this specific instantiation, the watermarks w_i can be thought of as visual patterns represented as "low-frequency (in comparison with the halftone frequency) images." Large font text rendered as a bi-level image is one example of such visual patterns.

Continuous phase-modulated halftoning[13] alters the halftone phase through a modulation of the phase of an underlying analytic halftone threshold function. This method has the benefit that the watermark pattern may be decided upon dynamically just prior to halftoning, as opposed to some of the alternate embedding strategies where the pattern must be incorporated in the design of the halftone thresholds and is therefore static. For completeness, we briefly summarize the embedding process here in our specific context of color halftoning. The halftone for the i^{th} separation, $I_i^h(x,y)$ is assumed to be obtained by comparing the contone image values $I_i(x,y)$ against a periodic halftone threshold function $T_i(x,y)$. Specifically

$$I_i^h(x,y) = \begin{cases} 1 & \text{if } I_i(x,y) < T_i(x,y), \\ 0 & \text{otherwise,} \end{cases} \tag{8}$$

where x and y represent the spatial coordinates along the horizontal and vertical directions, respectively.

In order to describe our watermark embedding technique, we use a modified version of the analytic description proposed by Pellar and Green.[20,21] We assume that the C, M, Y, and K separations have halftone frequencies of f^C, f^M, f^Y, and f^K lpi, and are oriented along angles ϕ^C, ϕ^M, ϕ^Y, and ϕ^K, respectively*. and the corresponding threshold function for the i^{th} separation is

$$T_i(x,y) = \cos\left(2\pi \frac{f^i}{\sqrt{2}} x'\right) \cos\left(2\pi \frac{f^i}{\sqrt{2}} y'\right), \tag{9}$$

*This description assumes orthogonal halftones, where the matrix of frequency vectors for each halftone separation is composed of two orthogonal vectors of equal length. More general descriptions are possible.[17]

where

$$\begin{bmatrix} x' \\ y' \end{bmatrix} = \begin{bmatrix} \cos\left(\phi^i - \frac{\pi}{4}\right) & -\sin\left(\phi^i - \frac{\pi}{4}\right) \\ \sin\left(\phi^i - \frac{\pi}{4}\right) & \cos\left(\phi^i - \frac{\pi}{4}\right) \end{bmatrix} \begin{bmatrix} x \\ y \end{bmatrix}. \tag{10}$$

A watermark pattern is embedded in the halftone by modulating the phase of one of the cosine function arguments by incorporating a spatially varying phase function $\Psi_i(x, y)$ such that phase variations are allowed along the respective halftone frequency direction. The modified version of the halftone threshold function is given by

$$T_i(x, y) = \cos\left(2\pi \frac{f^i}{\sqrt{2}} x' + \Psi_i(x, y)\right) \cos\left(2\pi \frac{f^i}{\sqrt{2}} y'\right). \tag{11}$$

Discontinuities in the phase term Ψ_i may produce visible artifacts in the halftone separation. Continuity and smoothness of this term need to be ensured to prevent these artifacts. We therefore refer to the technique as continuous phase modulation (CPM). A visual watermark pattern such as a bi-level text image serves as the watermark based on which the phase modulation term Ψ_i for the i^{th} halftone separation is determined. Typically, the bi-level watermark is smoothed using a spatial blur to ensure continuity of the phase and the resulting values are normalized between $(0, \pi]$ to introduce a phase change of π radians between the two levels of the watermarked image, which results in maximal contrast for the detected watermark pattern.[13]

The digitally embedded watermark pattern can be retrieved by overlaying the printed halftone image with an appropriate "decoder mask". In has been analytically demonstrated that the visible pattern after this overlay resembles the embedded watermark pattern, which allows visual detection.[13] This operation is digitally simulated for the individual colorant halftone separation estimates to extract the watermark patterns.

5. EXPERIMENTAL RESULTS

Our experimental setup utilized an electrophotographic CMYK color printer with an addressability of 600×600 dpi.

Stable moiré-free frequency vector configurations are sought in order to prevent self-detection.[14] For this purpose, we used the frequency vector configuration shown in Fig. 12 that are the scaled versions of the frequency vectors described by Schoppmeyer.[22] In each of the C, M, Y, and K colorant channels, a watermark pattern was embedded via the CPM method with maximum phase deviation $\kappa = \pi$.

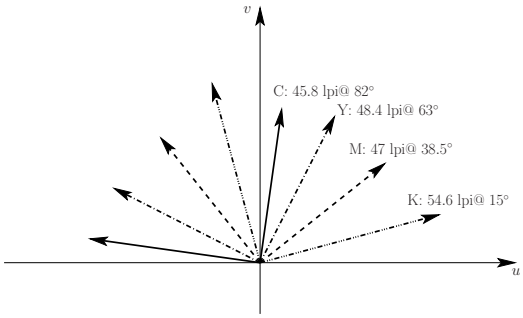

Figure 12. Frequency vectors for stable moiré-free C, M, Y, and K halftone screens.

The resulting color halftone is printed on our test printer and scanned with a flatbed RGB scanner with optical resolution of 600×600 dpi. Estimates of C, M, Y, and K halftones are obtained according to Eq. (4) from, respectively, the R, G, and B channels of the scanned image. The band-reject filters designed for the frequency vectors shown in Fig. 12 are shown in Fig. 13. Estimated halftone separations are then overlaid with the corresponding decoder masks to recover the embedded watermark patterns.

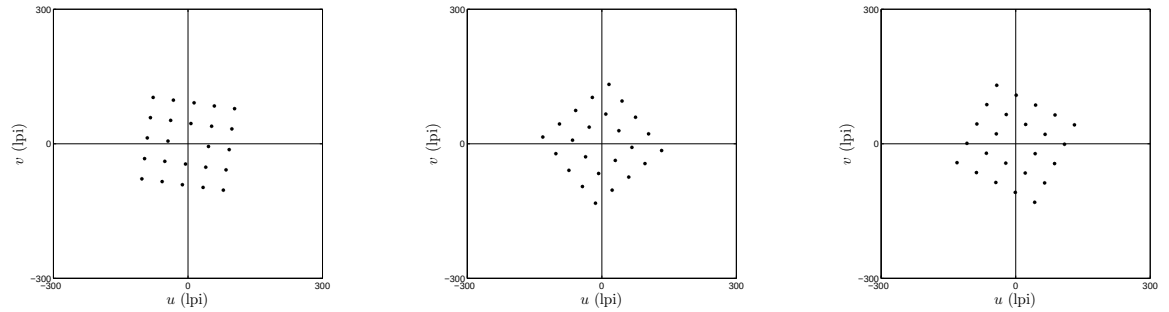

(a) $H_C(u,v)$ (b) $H_M(u,v)$ (c) $H_Y(u,v)$

Figure 13. Narrow band-reject filters for eliminating the CMY frequency components from the RGB channels of the scanned images for the frequency vector configuration shown in Fig. 12.

We illustrate the operation of the proposed methodology by using the *Hats* image shown in Fig. 10(a). For our experiment, we embedded the watermark patterns shown in Fig. 14 in our C, M, Y, and K halftone channel separations. Fig. 15 shows the detection results obtained for our example. The watermark pattern in each separation are visible in the regions, where they are embedded. The analysis for the detectability of the embedded watermark pattern indicates watermarks embedded in the midtones can be detected much easier than the watermarks embedded in the highlights and shadows.[13] This effect is particularly observed in Y and K channels, since Y channel of the *Hats* image includes many dark regions with near 100% coverage and K channel includes many bright regions with near 0% coverage, which do not allow for meaningful watermark embedding and extraction due to the absence of halftone structure.

(a) w_C (b) w_M (c) w_Y (d) w_K

Figure 14. Watermark patterns for C, M, Y, and K colorant separations.

(a) Cyan (b) Magenta (c) Yellow (d) Black

Figure 15. Detection results on the estimated halftone separations from the scanned RGB channel images. Artifacts due to re-screening in the printing process may not allow clear observation of the detected watermark pattern in the printed version of these figures. Please refer to the electronic version of this paper to clearly observe the detection results.

6. CONCLUSION

In this paper, we propose a methodology to embed watermark patterns in clustered-dot color halftones on per-channel basis. We demonstrate that by exploiting spatial frequency separability of clustered-dot color halftones, estimates of the individual colorant halftone separations can be obtained from scanned RGB images allowing for

per-channel detection to operate effectively. Our simulation-based evaluations indicate satisfactory estimation accuracies (mostly above 90%) for the individual CMYK halftone separations. We also demonstrated the efficacy of this methodology using continuous phase modulation for the embedding of per-separation watermarks.

REFERENCES

[1] Cox, I., Miller, M., Bloom, J., Fridrich, J., and Kalker, T., [*Digital Watermarking and Steganography*], Morgan Kaufmann Publishers, San Francisco, CA, USA, second ed. (2007).

[2] "Special issue on digital watermarking," *IEEE Sig. Proc. Mag.* **17** (Sept. 2000).

[3] van Renesse, R. L., [*Optical Document Security*], Artech House, Boston, MA, third ed. (2005).

[4] Amidror, I., Chosson, S., and Hersch, R. D., "Moiré methods for the protection of documents and products: A short survey," *Journal of Physics: Conference Series* **77**(1), 012001 (2007).

[5] Briquet, C. M., [*Les Filigranes: Dictionaire Histoire Des Marques Due Papier Des Leur Appartion Vers 1282, Jusquen 1600*], Leipzig, second ed. (1923).

[6] Wang, S. and Knox, K. T., "Embedding digital watermarks in halftone screens," in [*Proc. SPIE: Security and Watermarking of Multimedia Contents II*], Wong, P. W. and Delp, E. J., eds., **3971**, 218–227 (Jan. 2000).

[7] Amidror, I., "New print-based security strategy for the protection of valuable documents and products using moiré intensity profiles," in [*Proc. SPIE: Optical Security and Counterfeit Deterrence Technique IV*], van Renesse, R. L., ed., **4677**, 89–100 (Jan. 2002).

[8] Sharma, G. and Wang, S., "Show-through watermarking of duplex printed documents," in [*Proc. SPIE: Security, Steganography, and Watermarking of Multimedia Contents VI*], Delp, E. J. and Wong, P. W., eds., **5306**, 670–684 (Jan. 2004).

[9] Liu, C., Wang, S., and Xu, B., "Authenticate your digital prints with Glossmark images," in [*Proceedings IS&T NIP20: International Conference on Digital Printing Technologies*], 312–316 (Oct. 2004).

[10] Bulan, O., Monga, V., Sharma, G., and Oztan, B., "Data embedding in hardcopy images via halftone-dot orientation modulation," in [*Proc. SPIE: Security, Forensics, Steganography, and Watermarking of Multimedia Contents X*], Delp, E. J., Wong, P. W., Dittmann, J., and Memon, N. D., eds., **6819**, 68190C–1–12 (Jan. 2008).

[11] Hains, C. M., Wang, S., and Knox, K. T., "Digital color halftones," in Sharma.[23] Chapter 6.

[12] Bulan, O., Monga, V., and Sharma, G., "High capacity color barcodes using dot orientation and color separability," in [*Proc. SPIE: Media Forensics and Security XII*], III, E. J. D., Dittmann, J., Memon, N. D., and Wong, P. W., eds., **7541**, 725417–1–7 (Jan. 2010).

[13] Oztan, B. and Sharma, G., "Continuous phase-modulated halftones," *IEEE Trans. Image Proc.* **18**, 2718–2734 (Dec. 2009).

[14] Oztan, B. and Sharma, G., "Clustered-dot color halftone watermarks," in [*Proc. IS&T/SID Sixteenth Color Imaging Conference: Color Science and Engineering: Systems, Technologies, Applications*], 99–104 (10-15 Nov. 2008).

[15] Yule, J. A. C., [*Principles of color reproduction, applied to photomechanical reproduction, color photography, and the ink, paper, and other related Industries*], Wiley, New York (1967).

[16] Kermisch, D. and Roetling, P., "Fourier spectrum of halftone images," *J. Opt. Soc. Am.* **65**, 716–723 (Jun. 1975).

[17] Oztan, B., Sharma, G., and Loce, R. P., "Misregistration sensitivity in clustered-dot color halftones," *J. Electronic Imaging* **17**, 023004,1–30 (Apr./Jun. 2008).

[18] Sharma, G., "Color fundamentals for digital imaging," in *Digital Color Imaging Handbook*.[23] Chapter 1.

[19] Gustavson, S., "Color gamut of halftone reproduction," *J. Imaging Sci. and Tech.* **41**, 283–290 (May/Jun. 1997).

[20] Pellar, R. J. and Green, L., "Electronic halftone generator." United States Patent No. 4149183 (1979).

[21] Pellar, R. J., "Electronic halftone generator." United States Patent No. 4196451 (1980).

[22] Schoppmeyer, J., "Screen systems for multicolor printing." United States Patent No. 4537470 (1985).

[23] Sharma, G., ed., [*Digital Color Imaging Handbook*], CRC Press, Boca Raton, FL (2003).